



Dragonfly Imaging of the Galaxy NGC 5907: A Different View of the Iconic Stellar Stream

Pieter van Dokkum¹, Colleen Gilhuly², Ana Bonaca³, Allison Merritt⁴, Shany Danieli^{1,5}, Deborah Lokhorst²,
Roberto Abraham², Charlie Conroy³, and Johnny P. Greco⁶

¹ Astronomy Department, Yale University, 52 Hillhouse Avenue, New Haven, CT 06511, USA

² Department of Astronomy & Astrophysics, University of Toronto, 50 St. George Street, Toronto, ON M5S 3H4, Canada

³ Harvard-Smithsonian Center for Astrophysics, 60 Garden Street, Cambridge, MA, USA

⁴ Max-Planck-Institut für Astronomie, Königstuhl 17, D-69117 Heidelberg, Germany

⁵ Physics Department, Yale University, 52 Hillhouse Avenue, New Haven, CT 06511, USA

⁶ Center for Cosmology and AstroParticle Physics (CCAPP), The Ohio State University, Columbus, OH 43210, USA

Received 2019 June 26; revised 2019 August 30; accepted 2019 September 3; published 2019 September 24

Abstract

In 2008 it was reported that the stellar stream of the edge-on spiral NGC 5907 loops twice around the galaxy, enveloping it in a giant corkscrew-like structure. Here we present imaging of this iconic object with the Dragonfly Telephoto Array, reaching a 1σ surface brightness level of $\mu_g = 30.3$ mag arcsec⁻² on spatial scales of $1'$ (the approximate width of the stream). We find a qualitatively different morphology from that reported in the 2008 study. The Dragonfly data do not show two loops but a single curved stream with a total length of $45'$ (220 kpc). The surface brightness of the stream ranges from $\mu_g \approx 27.6$ mag arcsec⁻² to $\mu_g \approx 28.8$ mag arcsec⁻², and it extends significantly beyond the region where tidal features had previously been detected. We find a density enhancement near the luminosity-weighted midpoint of the stream which we identify as the likely remnant of a nearly disrupted progenitor galaxy. A restricted N -body simulation provides a qualitative match to the detected features. In terms of its spatial extent and stellar mass the stream is similar to Sagittarius, and our results demonstrate the efficacy of low surface brightness-optimized telescopes for obtaining maps of such large streams outside the Local Group. The census of these rare, relatively high mass events complements the census of common, low-mass ones that is provided by studies of streams in the Milky Way halo.

Unified Astronomy Thesaurus concepts: Tidal disruption (1696); Dwarf galaxies (416); Low surface brightness galaxies (940)

1. Introduction

Stellar streams, the debris of tidally disrupted globular clusters or galaxies, provide information on the frequency of the accretion of small objects onto larger ones (see, e.g., Bullock & Johnston 2005). As their morphologies reflect their orbits they are also probes of the gravitational potential, and they have been used as a tool to constrain the mass and structure of dark matter halos (Moore et al. 1999; Ibata et al. 2002; Helmi 2004; Law & Majewski 2010; Bovy et al. 2017; Bonaca & Hogg 2018).

In the Milky Way dozens of stellar streams have been identified (see Grillmair & Carlin 2016; Shipp et al. 2018), with Sagittarius (Ibata et al. 1997), Palomar 5 (Odenkirchen et al. 2001), Monoceros (Newberg et al. 2002), and the “orphan stream” (Belokurov et al. 2007) among the most prominent examples. The number of confirmed and candidate streams is increasing rapidly, thanks to the increased contrast attainable with *Gaia* and deep star count maps (see, e.g., Malhan et al. 2018; Bonaca et al. 2019). Likewise, M31 is home to many tidally disrupting satellite objects, ranging from low-mass “stretched” objects such as Andromeda XIX (McConnachie et al. 2008) to the major event, or events, that were responsible for shaping the complex structure of the M31 halo (D’Souza & Bell 2018, and references therein).

At distances $D \gtrsim 5$ Mpc streams can be identified by the smooth integrated light of their stellar populations (e.g., Arp 1966; Malin & Hadley 1997; Mihos et al. 2005; van Dokkum 2005; Bell et al. 2006; Martínez-Delgado et al. 2010; Atkinson et al. 2013). Such integrated-light measurements typically do not reach the same stellar density limits as star

count surveys but probe a much greater volume of the universe (see Danieli et al. 2018 for a quantitative discussion). The combination of studies of frequent, low-mass-accretion events in the Local Group with systematic integrated-light surveys of rare, high-mass events around other galaxies should ultimately provide a complete census of present-day accretion-driven galaxy growth.

One of the best-known tidal features outside of the Local Group is the stellar stream associated with NGC 5907, an edge-on spiral galaxy with a stellar mass of $\approx 8 \times 10^{10} M_\odot$ (Laine et al. 2016) at a distance of 17 Mpc (Tully et al. 2016). The stream was discovered by Shang et al. (1998) and Zheng et al. (1999), who detected sections of a loop around the disk of NGC 5907 using the Beijing Astronomical Observatory 0.6/0.9 m Schmidt telescope. This was a remarkable discovery, as previous deep optical and HI searches had not uncovered any tidal features associated with NGC 5907 (see Sancisi 1976; Sasaki 1987; Sackett et al. 1994). The galaxy was subsequently imaged by Martínez-Delgado et al. (2008, hereafter M08), using a 0.5 m Ritchey–Chrétien telescope. M08 report that the stream exhibits not one but two complete loops, enveloping NGC 5907 in a giant corkscrew-like structure. Their evocative image, whose main features could be reproduced with an N -body model, has taken on an iconic status, serving as a powerful demonstration of the shredding of a small galaxy.⁷ Some years later NGC 5907 was also observed by Laine et al. (2016), who combined data from the *Spitzer Space Telescope*

⁷ We note that Wang et al. (2012) interpret the M08 data as evidence of a major merger.

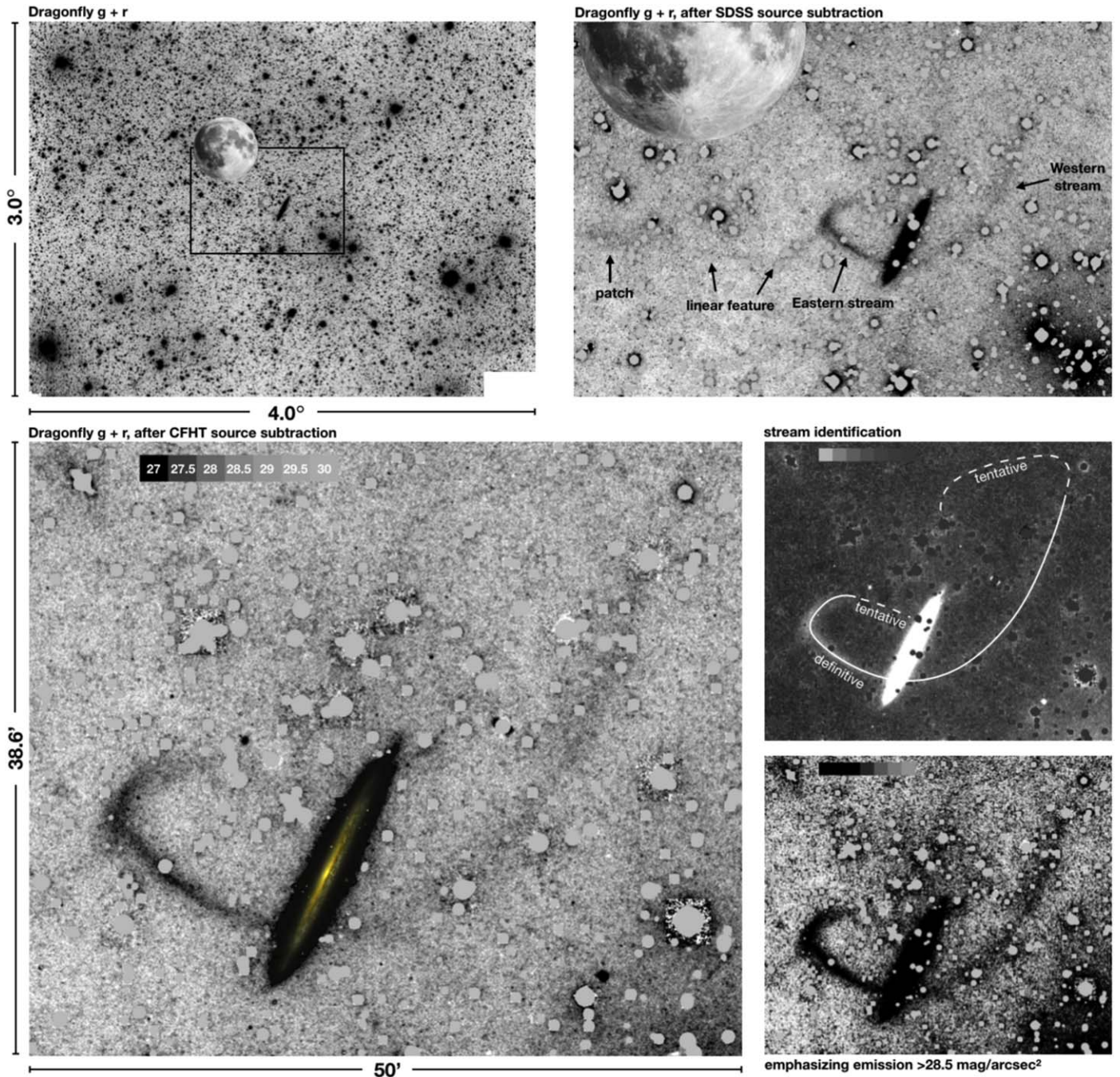


Figure 1. Dragonfly imaging of the NGC 5907 field, with north up and east to the left. Top left: sum of the g - and r -band images. Top right: zoom on the vicinity of NGC 5907, after subtracting a model of compact emission in the frame. The image shows a single coherent stellar stream with a length of $\approx 45'$ that crosses the galaxy. We also identify a thin, linear feature to the east and a low surface brightness patch 1° from NGC 5907. Bottom panels: the region of the NGC 5907 stream, at three different scalings. The scale bar at the top indicates the surface brightness in AB mag arcsec $^{-2}$.

with optical Subaru images. These authors studied the part of the stream that was detected by Shang et al. (1998) and do not comment on the second loop that was reported by M08.

Here we report on new low surface brightness imaging of NGC 5907 over a wide field, as part of an imaging campaign of nearby galaxies with the Dragonfly Telephoto Array (Abraham & van Dokkum 2014). We are conducting two surveys, the Dragonfly Nearby Galaxies Survey (Merritt et al. 2016) and the Dragonfly Edge-on Galaxies Survey (C. Gilhuly et al. 2019, in preparation); NGC 5907 was one of the first targets of the edge-on survey.

2. Data

2.1. Observations and Reduction

The observations were obtained with the Dragonfly Telephoto Array, a low surface brightness-optimized telescope consisting of 48 Canon 400 mm $f/2.8$ II telephoto lenses. Its basic design is described in Abraham & van Dokkum (2014), Merritt et al. (2016), and Zhang et al. (2018). The current 48-lens array is described in S. Danieli et al. (2019, in preparation). Briefly, each lens is coupled to an SBIG STT-8300M camera offering a 2.6×1.9 instantaneous field of

view with $2''.8$ native pixels and an FWHM spatial resolution of $\approx 6''.7$. The lenses are intentionally offset from one another by $\approx 10\%$ of the field of view, giving 48 independent sightlines. Data are taken with large ($\approx 25'$) dithers between exposures, providing further redundancy. As the data are sky-limited in our 600 s integrations the telescope behaves optically like a 1.0 m $f/0.4$ refractor with superb optical surfaces and near-perfect baffling. Twenty-four lenses are equipped with Sloan Digital Sky Survey (SDSS) g filters and 24 with SDSS r filters.

The data reduction is gate-based, executing multiple quality tests on each frame as it progresses through the pipeline. The background modeling is done in two stages. After the first stage a mask is generated containing all detected emission in the coadded image. This is used in the second stage to mask all emission sources from the individual raw frames prior to fitting the background with a two-dimensional third-order polynomial. In this step variation on scales exceeding $\sim 0''.9 \times 0''.6$ is removed; features that are smaller in at least one dimension (such as the stellar stream, which has a width of $\approx 0''.02$) remain unaffected. The pipeline is described in detail in Zhang (2018) and in S. Danieli et al. (2019, in preparation). The total number of frames that went into the final NGC 5907 stacks is 618 in g and 762 in r ; this is the equivalent of 4.8 hr with the full 48 lens array. The summed $g + r$ image is shown in the top left of Figure 1; owing to the dithering it covers 12 degree^2 , with reduced effective exposure time near the edges of the field.

2.2. Multiresolution Filtering

The Dragonfly data have excellent low surface brightness sensitivity and are essentially free of ghosts, reflections, and other artifacts. However, they suffer from crowding due to the relatively low spatial resolution. We subtracted compact emission sources from the data using multiresolution filtering. Details are given in van Dokkum et al. (2019). Briefly, a flux model is created by multiplying an image of higher resolution (such as archival Canada–France–Hawaii Telescope (CFHT) data) by a SExtractor (Bertin & Arnouts 1996) object map of that image. Any detected low surface brightness features in the high-resolution data can be removed from the model at this stage. The model is then convolved with a kernel to match the Dragonfly resolution and subtracted. Remaining halos around bright stars are removed following a similar process as described in van Dokkum et al. (2014). The point-spread function is modeled in a $2''.0 \times 2''.0$ box; this is generally sufficient but we note that the very brightest stars have detected light at larger radii in the residual image.

The results are shown in Figure 1. For the image at top right the high-resolution model was created from SDSS g and r images. These are shallow but have few artifacts and enable a wide field subtraction. The images in the bottom panels were filtered using a combination of CFHT and Beijing–Arizona All Sky Survey (BASS; Zou et al. 2018) imaging. The BASS data are only used to identify and remove artifacts and missing data in the CFHT images. We carefully checked that no low surface brightness emission is contained in the high-resolution model. The only low surface brightness object that we removed from the model is a previously uncataloged dwarf galaxy.

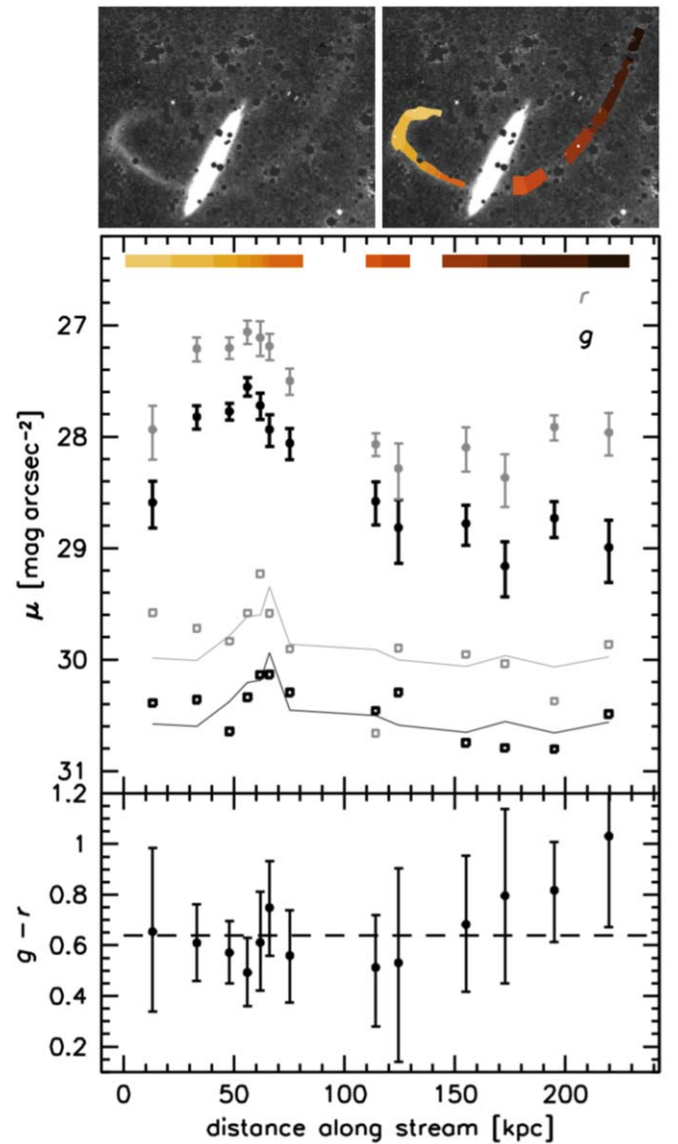


Figure 2. Photometry along the stream. Top panel: g - and r -band surface brightness. Open symbols indicate the 1σ uncertainty (see the text). The average surface brightness of the stream is $\mu_g \approx 27.8$ on the east side of the galaxy and $\mu_g \approx 28.8 \text{ mag arcsec}^{-2}$ on the west side. Bottom panel: $g - r$ color along the stream, with the mean indicated by the dashed line.

3. Observational Results

3.1. Morphology and Photometry of the Stream

The Dragonfly images show a relatively straightforward stream morphology. We confirm the existence of the strongly curved eastern stream that was discovered by Shang et al. (1998) (see top right panel of Figure 1). We find that the stream continues on the west side of NGC 5907 at lower surface brightness. This western stream reaches more than twice the length of the eastern stream. This stream morphology is qualitatively different from the double loop structure reported by M08; we return to this in Section 5. We also detect a thin feature extending from the brightest part of the stream to the east and a faint patch about 1° due east of NGC 5907. These faint features are not artifacts and are seen in both g and r ; their nature is unclear. Finally, we tentatively detect continuations of the

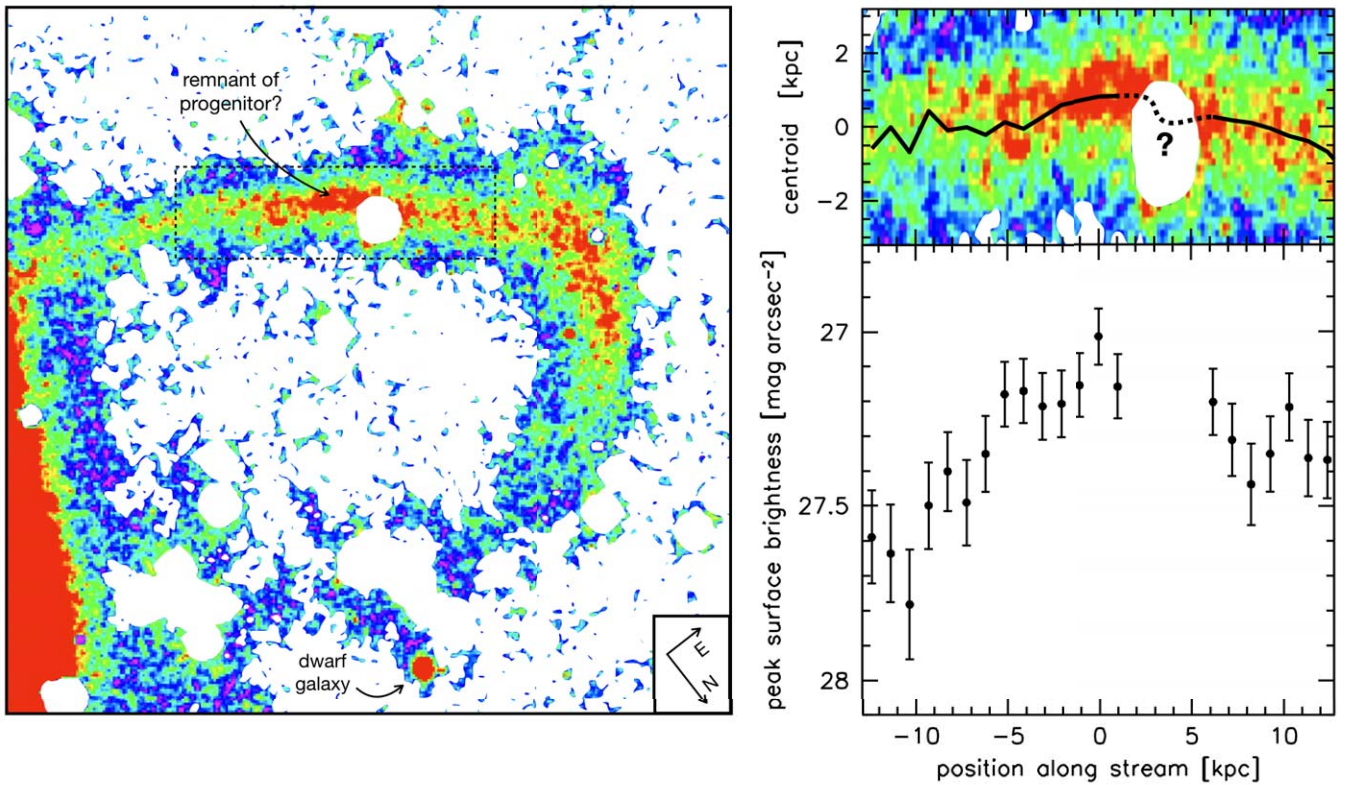


Figure 3. Left: false-color image of the eastern stream, rotated by 142° . Right: results of Gaussian fits in $12''/5$ bins along the stream segment shown in the box at the left. The top panel shows the best-fit position, and the bottom panel shows the surface brightness of the peak of the Gaussian. There is a clear stellar density enhancement in this region, and a possible asymmetry.

stream at both ends: there may be a thin extension of the western stream toward the northeast, looping back south toward the disk, and there is a likely continuation of the eastern stream toward the disk. Both these extensions are labeled “tentative” in Figure 1, and they are not included in our analysis.

The surface brightness along the stream in g and r is quantified using aperture photometry. The apertures aim to include most of the width of the stream. As shown in Figure 2 the surface brightness reaches a peak of $\mu_g \approx 27.6$ mag arcsec $^{-2}$ on the east side of the galaxy. On the west side the surface brightness is lower at $\mu_g \approx 28.8$ mag arcsec $^{-2}$. The uncertainties in the data points are determined by moving the apertures off of the actual stream and then obtaining fluxes in these “empty” locations. The apertures retain their position relative to each other, with the entire set of stream apertures moved to 52 different positions. In 13 of these positions the stream has the same orientation as the actual stream; in the other sets of positions it is flipped in x , y , and both x and y . The 1σ variation in these measurements is taken as the uncertainty (open symbols in Figure 2). These uncertainties are not constant along the stream, as they depend on the size of the photometric aperture: for the larger apertures on the western side the uncertainties are smaller than for the smaller apertures on the eastern side. From a fit to the empirically determined uncertainties we find that

$$\sigma(\mu_g) \approx 30.25 + 0.5 \log(A) \quad (1)$$

and

$$\sigma(\mu_r) \approx 29.66 + 0.5 \log(A), \quad (2)$$

with A the aperture size in arcmin 2 (thin lines). The $g - r$ color along the stream is shown in the bottom panel. The data

are consistent with a constant color along the stream of $\langle g - r \rangle \approx 0.64 \pm 0.11$ mag (where the error bar is the combination of ± 0.04 random and ± 0.1 mag systematic uncertainty). These results are broadly consistent with Shang et al. (1998) and Laine et al. (2016), who obtained photometry for the relatively bright eastern part of the stream only.

The total magnitudes integrated over all apertures are $m_g = 15.5$ and $m_r = 14.8$. There are two gaps in the photometric apertures: one coinciding with the disk and another with a bright star (see the top right panel of Figure 2). Interpolating over these apertures suggests these regions contain $\approx 10\%$ of the light of the stream. Assuming another 10% is missed in regions that are fainter than our detection limit, we estimate that the total magnitudes of the stream are $m_g \approx 15.3$ and $m_r \approx 14.6$. For $D = 17$ Mpc this corresponds to $L_g \approx 1.8 \times 10^8 L_\odot$. For an analysis of the stellar population of the stream we refer the reader to Laine et al. (2016).

3.2. Probable Identification of the Progenitor Galaxy

Stellar streams are generated by mass loss from a progenitor object along its orbit. Generally the progenitor object is within the densest part of the stream, is near the luminosity-weighted midpoint of the stream, and coincides with a displacement (as the leading and trailing streams come from stars that became unbound at opposite Lagrange points, toward the center and anticenter of the potential). These are not absolutes, as the orbital geometry, the superposition of successive passages, and projection effects complicate the observed morphology.

We identify the likely remnant of the progenitor object within the region highlighted in the left panel of Figure 3. In

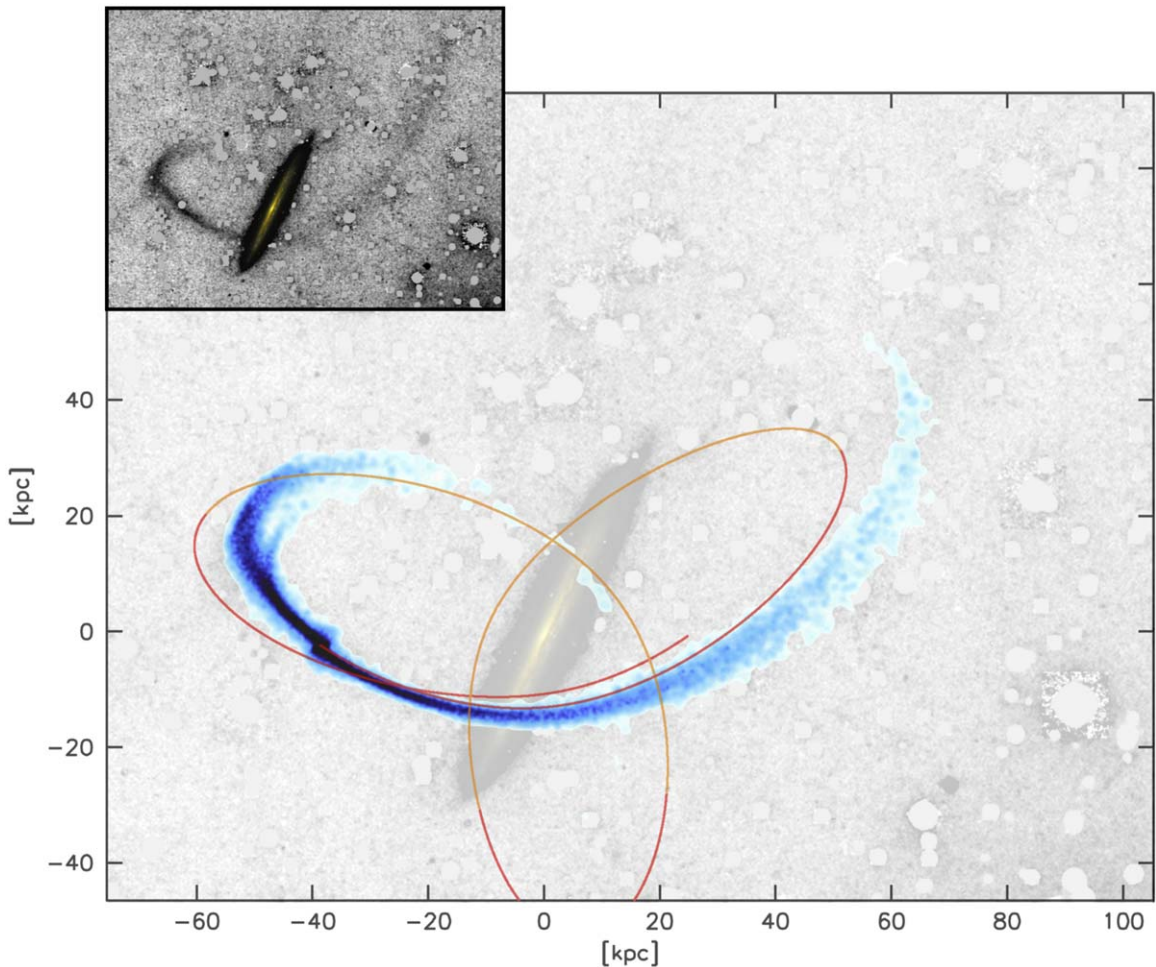


Figure 4. Restricted N -body simulation of a disrupting galaxy with a mass of $2 \times 10^8 M_{\odot}$, with its present-day location matched to that of the progenitor identified in Section 3.2. The line indicates the most recent 2.5 Gyr of the orbit, with red and orange alternating every 0.5 Gyr.

the right panel we show the centroid of the emission and the peak brightness as a function of the position along this stream segment. These values are determined by fitting Gaussians to the stream profile (i.e., in the vertical direction in Figure 3), averaging the $g+r$ emission in $12''.5$ sections along the stream. There is a peak in the surface brightness close to the luminosity-weighted midpoint of the stream: $\sim 40\%$ of the luminosity is to the east and $\sim 60\%$ to the west. Furthermore, the centroid shows several ~ 1 kpc sized offsets that could indicate the characteristic displacement of the leading and trailing streams. A possible location is indicated with the broken line and the question mark; unfortunately it coincides with a bright foreground star.

4. Dynamical Stream Model

In this section we show that a tidally disrupting satellite reproduces the overall stream morphology and the identified location of the progenitor. We followed the methodology developed for modeling streams in the Milky Way (e.g., Price-Whelan & Bonaca 2018), and started by rotating the coordinate system such that the galaxy is aligned with the x -axis, z is perpendicular to the disk plane, and y is the radial direction. The gravitational potential is set up with the same assumptions as M08 used for the disk (mass: $8.4 \times 10^{10} M_{\odot}$, scale length: 6.24 kpc, scale height: 0.26 kpc) and bulge (mass: 2.3×10^{10}

M_{\odot} , scale radius: 0.6 kpc). We used a more massive halo than M08 (mass: $1.2 \times 10^{12} M_{\odot}$, scale radius: 26 kpc, and z -axis flattening of 1.1) to better match the recent rotation curve measurement of Posti et al. (2019); we tested that the M08 halo also leads to a good match to the observed stream.

With the potential in place, we searched for the 6D location of the progenitor until we obtained an orbit that approximately matches the detected stream positions. The progenitor is assumed to be at the approximate x, z position determined in Section 3.2, and for simplicity we set $y = 0$. The velocity is tweaked in the positive x, z direction, as the morphology suggests that the eastern stream is the leading tail. In our model, the progenitor is currently at $\mathbf{x} = (-19.0, 0.0, 33.8)$ kpc, $\mathbf{v} = (30, 65, 225)$ km s $^{-1}$. Due to projection effects and the lack of kinematic data this solution is not unique, but we leave a full exploration of the parameter space to future work.

With the orbit determined, we created a mock stream using the Fardal et al. (2015) method implemented in the *gala* package (Price-Whelan 2017). During the most recent 2.5 Gyr of the orbit we released tracer particles from the progenitor, tuning the spatial and kinematic offsets of the escaping stars to best represent the shape of the observed stream close to the progenitor. The progenitor initially had a stellar mass of $2 \times 10^8 M_{\odot}$.

The orbit and mock stream are shown in Figure 4. There are discrepancies on small scales; however, the model reproduces the overall path, the higher density of the leading (eastern) tail,

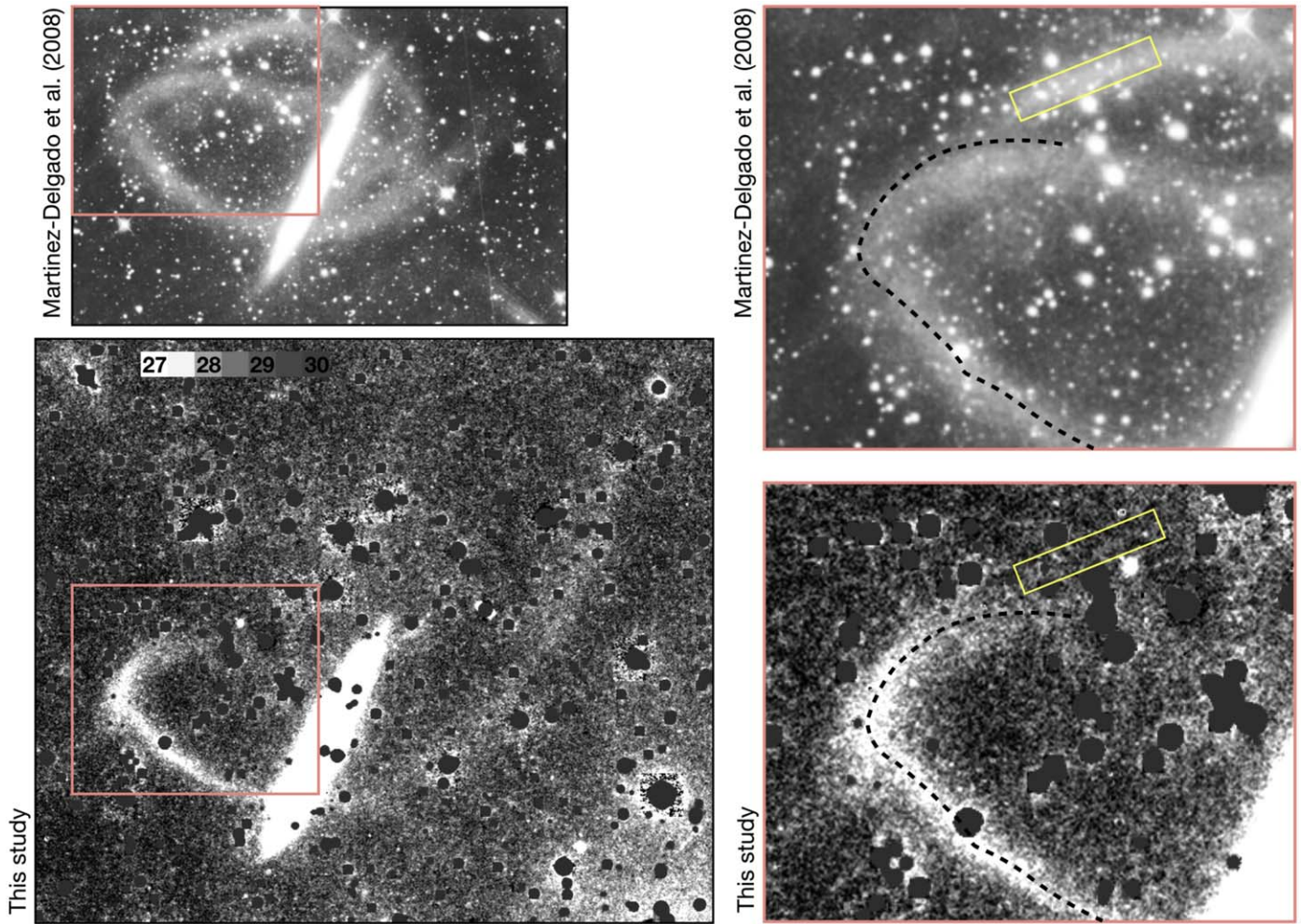


Figure 5. Comparison of the stream morphology in **M08** and in the Dragonfly $g + r$ image. We do not confirm the presence of a second loop. The yellow box indicates the brightest part of the entire **M08** stream system; our limit is $\mu_g > 29.4 \text{ mag arcsec}^{-2}$ in that region. Furthermore, the first loop is in a different location, as indicated by the black broken line.

and the asymmetric broadening of the leading tail where it curves back toward NGC 5907.

5. Discussion

In this Letter we present Dragonfly imaging of the NGC 5907 system, focusing on its well-known stellar stream. We find a relatively straightforward system composed of the remnant of a progenitor galaxy, a leading tail, and a long faint trailing tail. This overall morphology can be reproduced with a dynamical model without much fine-tuning. In terms of its spatial extent and stellar mass the stream is similar to the Sagittarius stream (see Sesar et al. 2017). The Milky Way and NGC 5907 are also quite similar, which means that the entire system offers an interesting analog to this accretion event.

We now turn to the most puzzling aspect of our study. As shown in Figure 5 the morphology of the stream in our data is qualitatively different from that reported by **M08**. First, we do not confirm the presence of a second (northern) loop, even though it contains the brightest part of the entire **M08** tidal stream system. This stream segment is indicated by the $1' \times 5'$ yellow box in Figure 5. From Equation (1) we determine a 3σ upper limit of $\mu_g > 29.4 \text{ mag arcsec}^{-2}$ for this region. Second, the first loop is in a different place: the location in the Dragonfly image falls *in between* the two loops identified in **M08** (see

Figure 5). Other discrepancies are a greater length of the western stream in our data, the presence of a density enhancement in the first loop (which we identify as the location of the progenitor), and the much smaller ratio of the apparent width of the stream to the apparent width of the NGC 5907 disk.









It is unlikely that these discrepancies are caused by a difference in depth or by color variation along the stream. The **M08** image was obtained by an amateur astronomer in close coordination with professional astronomers, using a 0.5 m telescope located on the same site as Dragonfly. The limiting surface brightness of the **M08** image should approach that of the Dragonfly image when the size of the telescope, the exposure time (5.8 hr in white light and 5.6 hr in red, green, and blue filters), and the throughput of the filters are taken into account. Furthermore, neither a difference in depth nor a color gradient can explain the different locations of the first loop and the other qualitative discrepancies between the two data sets. We note that other images of NGC 5907 in the literature appear to show only one loop in the same location as in the Dragonfly data (see Shang et al. 1998; Miskolczi et al. 2011; Lang et al. 2014; Laine et al. 2016). We provide our data on a web page so that others can assess them.⁸

⁸ See <https://www.pietervandokkum.com/ngc5907>.

There are several routes to make further progress. Deeper data can verify the reality of the tentative sections of the stream and better quantify its substructure. We will also search for streams around other galaxies, both in targeted surveys (Merritt et al. 2016; C. Gilhuly et al. 2019, in preparation) and in blank field surveys (S. Danieli et al. 2019, in preparation). More generally, this study follows previous work in demonstrating the power of the combination of low surface brightness imaging with dynamical modeling (see also, e.g., Foster et al. 2014; Amorisco et al. 2015; Pearson et al. 2019). Systematic surveys of accretion events across the nearby universe are providing complementary information to the extensive work in the Local Group.

We thank Stefan Binnewies, Josef Pöpsel, and Dieter Beer for their help in understanding their images of NGC 5907, and the referee for insightful comments that improved the manuscript. Support from NSF grant AST-1613582 is gratefully acknowledged.

ORCID iDs

Pieter van Dokkum  <https://orcid.org/0000-0002-8282-9888>
 Ana Bonaca  <https://orcid.org/0000-0002-7846-9787>
 Allison Merritt  <https://orcid.org/0000-0001-9467-7298>
 Shany Danieli  <https://orcid.org/0000-0002-1841-2252>
 Deborah Lokhorst  <https://orcid.org/0000-0002-2406-7344>
 Roberto Abraham  <https://orcid.org/0000-0002-4542-921X>
 Charlie Conroy  <https://orcid.org/0000-0002-1590-8551>
 Johnny P. Greco  <https://orcid.org/0000-0003-4970-2874>

References

- Abraham, R. G., & van Dokkum, P. G. 2014, *PASP*, 126, 55
 Amorisco, N. C., Martínez-Delgado, D., & Schedler, J. 2015, arXiv:1504.03697
 Arp, H. 1966, *ApJS*, 14, 1
 Atkinson, A. M., Abraham, R. G., & Ferguson, A. M. N. 2013, *ApJ*, 765, 28
 Bell, E. F., Naab, T., McIntosh, D. H., et al. 2006, *ApJ*, 640, 241
 Belokurov, V., Evans, N. W., Irwin, M. J., et al. 2007, *ApJ*, 658, 337
 Bertin, E., & Arnouts, S. 1996, *A&AS*, 117, 393
 Bonaca, A., Conroy, C., Price-Whelan, A. M., & Hogg, D. W. 2019, *ApJL*, 881, L37
 Bonaca, A., & Hogg, D. W. 2018, *ApJ*, 867, 101
 Bovy, J., Erkal, D., & Sanders, J. L. 2017, *MNRAS*, 466, 628
 Bullock, J. S., & Johnston, K. V. 2005, *ApJ*, 635, 931
 Danieli, S., van Dokkum, P., & Conroy, C. 2018, *ApJ*, 856, 69
 D'Souza, R., & Bell, E. F. 2018, *NatAs*, 2, 737
 Fardal, M. A., Huang, S., & Weinberg, M. D. 2015, *MNRAS*, 452, 301
 Foster, C., Lux, H., Romanowsky, A. J., et al. 2014, *MNRAS*, 442, 3544
 Grillmair, C. J., & Carlin, J. L. 2016, in *Tidal Streams in the Local Group and Beyond*, Astrophysics and Space Science Library Vol. 420, ed. H. J. Newberg & J. L. Carlin (Dordrecht: Springer), 87
 Helmi, A. 2004, *ApJL*, 610, L97
 Ibata, R. A., Lewis, G. F., Irwin, M. J., & Quinn, T. 2002, *MNRAS*, 332, 915
 Ibata, R. A., Wyse, R. F. G., Gilmore, G., Irwin, M. J., & Suntzeff, N. B. 1997, *AJ*, 113, 634
 Laine, S., Grillmair, C. J., Capak, P., et al. 2016, *AJ*, 152, 72
 Lang, D., Hogg, D. W., & Scholkopf, B. 2014, *PMLR*, 33, 549
 Law, D. R., & Majewski, S. R. 2010, *ApJ*, 714, 229
 Malhan, K., Ibata, R. A., & Martin, N. F. 2018, *MNRAS*, 481, 3442
 Malin, D., & Hadley, B. 1997, *PASA*, 14, 52
 Martínez-Delgado, D., Gabany, R. J., Crawford, K., et al. 2010, *AJ*, 140, 962
 Martínez-Delgado, D., Peñarrubia, J., Gabany, R. J., et al. 2008, *ApJ*, 689, 184
 McConnachie, A. W., Huxor, A., Martin, N. F., et al. 2008, *ApJ*, 688, 1009
 Merritt, A., van Dokkum, P., Abraham, R., & Zhang, J. 2016, *ApJ*, 830, 62
 Mihos, J. C., Harding, P., Feldmeier, J., & Morrison, H. 2005, *ApJL*, 631, L41
 Miskolczi, A., Bomans, D. J., & Dettmar, R. J. 2011, *A&A*, 536, 66
 Moore, B., Ghigna, S., Governato, F., et al. 1999, *ApJL*, 524, L19
 Newberg, H. J., Yanny, B., Rockosi, C., et al. 2002, *ApJ*, 569, 245
 Odenkirchen, M., Grebel, E. K., Rockosi, C. M., et al. 2001, *ApJL*, 548, L165
 Pearson, S., Starkeburg, T. K., Johnston, K. V., Williams, B. F., & Ibata, R. A. 2019, arXiv:1906.03264
 Posti, L., Fraternali, F., & Marasco, A. 2019, *A&A*, 626, 56
 Price-Whelan, A. M. 2017, *JOSS*, 2, 388
 Price-Whelan, A. M., & Bonaca, A. 2018, *ApJL*, 863, L20
 Sackett, P. D., Morrison, H. L., Harding, P., & Boroson, T. A. 1994, *Natur*, 370, 441
 Sancisi, R. 1976, *A&A*, 53, 159
 Sasaki, T. 1987, *PASJ*, 39, 849
 Sesar, B., Hernitschek, N., Dierickx, M. I. P., Fardal, M. A., & Rix, H.-W. 2017, *ApJL*, 844, L4
 Shang, Z., Zheng, Z., Brinks, E., et al. 1998, *ApJL*, 504, L23
 Shipp, N., Drlica-Wagner, A., Balbinot, E., et al. 2018, *ApJ*, 862, 114
 Tully, R. B., Courtois, H. M., & Sorce, J. G. 2016, *AJ*, 152, 50
 van Dokkum, P. G. 2005, *AJ*, 130, 2647
 van Dokkum, P. G., Abraham, R., Merritt, A., et al. 2014, *ApJL*, 782, L24
 van Dokkum, P., Lokhorst, D., Danieli, S., et al. 2019, *PASP*, submitted
 Wang, J., Hammer, F., Athanassoula, E., et al. 2012, *A&A*, 538, A121
 Zhang, J. 2018, PhD thesis, Univ. Toronto, http://jilaizhang.github.io/files/Zhang_Jielai_201811_PhD_Thesis_excludech4.pdf
 Zhang, J., Abraham, R., van Dokkum, P., Merritt, A., & Janssens, S. 2018, *ApJ*, 855, 78
 Zheng, Z., Shang, Z., Su, H., et al. 1999, *AJ*, 117, 2757
 Zou, H., Zhang, T., Zhou, Z., et al. 2018, *ApJS*, 237, 37